

# 光学学报

## 氮化硅片上光栅耦合器的优化和实验

冉娜, 陈昕阳, 汪正坤, 张洁\*

重庆大学光电技术及系统教育部重点实验室, 重庆 400044

**摘要** 在785 nm激励的拉曼片上传感器结构中, 氮化硅片上光栅耦合器的性能直接关系到激励光的耦合效果。首先建立了光栅耦合器的二维、三维结构模型, 采用时域有限差分(FDTD)仿真软件对光栅耦合器进行数值分析。以耦合效率为主要性能指标, 分析了光源入射角度、光栅常数、光栅高度、填充因子和光栅刻蚀深度各参数的影响。采用电子束光刻法制备了光栅耦合器。最后, 对三维全刻蚀聚焦波导光栅耦合器进行了测试。结果表明, 二维波导光栅耦合器的性能最好, 其耦合效率可达39.64%, 三维全刻蚀聚焦波导光栅耦合器在实际测试中的耦合效率能达19.91%。光栅耦合器能有效将光耦合进波导中, 在波导传感中具有潜在的应用。

**关键词** 集成光学; 光栅耦合器; 氮化硅波导; 结构优化; 耦合效率

中图分类号 TN26

文献标志码 A

DOI: 10.3788/AOS221307

### 1 引言

拉曼光谱检测系统片上化集成是目前拉曼光谱技术的研究热点, 其将波导与拉曼相结合<sup>[1-3]</sup>。其中, 有效地将激励光波耦合进波导对于拉曼光谱传感和信号采集尤其重要, 目前该过程主要采用波导光栅耦合器来实现。波导光栅耦合器主要分为直波导光栅耦合器和聚焦波导光栅耦合器两类。赵然等<sup>[4-5]</sup>设计了亚波长光栅耦合器, 其耦合效率高达90%。Sacher等<sup>[6]</sup>设计了一种对氮化硅和硅进行相间刻蚀的直波导光栅耦合器, 该光栅耦合器在C波段附近能实现高耦合效率, 耦合效率最高达-1.3 dB。Benedikovic等<sup>[7]</sup>设计了一种在220 nm厚的SOI(silicon-on-insulator)衬底上进行阵列刻蚀的直波导光栅耦合器, 该光栅耦合器在1550 nm和1300 nm波长附近分别实现了-1.97 dB和-1.61 dB的耦合效率。Gao等<sup>[8]</sup>设计了一种直硅波导光栅耦合器, 将其作为角度检测器, 检测角度范围为25°。Larrea等<sup>[9]</sup>通过半解析法设计了一种直硅波导光栅耦合器, 在1550 nm和1300 nm波长附近实现了50%的耦合效率。Hong等<sup>[10]</sup>设计了一种包括分段光栅的直硅波导光栅耦合器, 在1550 nm波长处实现了51.70%的耦合效率。Xu等<sup>[11]</sup>设计了一种增加金属膜和反射光栅的聚合物直波导光栅耦合器, 在1550 nm波长下, 其最高耦合效率为51.30%。van Laere等<sup>[12]</sup>设计了一种聚焦型波导光栅耦合器, 在1550 nm波段附近实现了20%的耦合效率。Zhao等<sup>[13]</sup>结合聚焦光

栅和逆锥度设计, 制备了聚焦波导光栅耦合器, 其在C波段的耦合效率为-3.7 dB。Cheng等<sup>[14]</sup>设计了一种可以工作在双波段的聚焦波导光栅耦合器, 在1310 nm和1490 nm波长附近分别实现了-5.86 dB和-4.26 dB的耦合效率。

现有的光栅耦合器大多都是对C波段进行研究, 且光栅耦合器结构设计较复杂, 制备工艺难度较大。由于氮化硅的透明窗口在400~3500 nm之间, 范围较宽<sup>[15]</sup>, 且氮化硅的折射率较为适中(约为2.3), 其与周围材料的大折射率差足以将光波的能量束缚在波导层中, 减小损耗。因此, 本文设计了氮化硅片上光栅耦合器, 激励光源为785 nm。该光栅耦合器结构简单, 制备工艺简单。以耦合效率为主要性能指标, 对直波导和聚焦波导均作了研究并进行了光栅耦合器测试实验, 这为研究785 nm波段附近的光栅耦合器提供了基础, 该光栅耦合器能将激励光有效地耦合进波导, 也为拉曼光谱传感和信号采集提供了有效的帮助。

### 2 原理

#### 2.1 基本原理

光栅耦合器是一种周期性结构, 激光通过光纤传输到光栅耦合器上方, 经过光栅作用后产生衍射输出光, 部分衍射光会耦合进波导中。常用布拉格公式来研究耦合过程<sup>[16]</sup>, 其表示了入射光波矢量与衍射光波矢量之间的关系, 布拉格公式为

$$\beta = k_{\text{inc}} + mk, \quad (1)$$

收稿日期: 2022-06-13; 修回日期: 2022-07-06; 录用日期: 2022-07-11; 网络首发日期: 2022-07-21

基金项目: 国家自然科学基金(62175023, 61875024)、重庆市杰出青年基金(cstc2019jcyjjqX0018)

通信作者: \*zhangjie@cqu.edu.cn

式中: $\beta$ 表示波导的传播常数; $k_{\text{inc}}$ 表示入射光的波数,且 $k_{\text{inc}}=2\pi n_1/(\lambda_0 \sin \theta)$ ( $\lambda_0$ 为入射光波长, $\theta$ 为光源入射角, $n_1$ 为空气折射率); $k$ 表示光栅矢量大小且 $k=2\pi/\Lambda$ , $\Lambda$ 为光栅常数; $m$ 为衍射级次( $m=\pm 0, \pm 1, \pm 2, \dots$ )。

二维光栅耦合器的结构如图1所示,上层是折射

率为 $n_1=1$ 的空气,波导层是折射率为 $n_2=2.3$ 的氮化硅,衬底是折射率为 $n_3=1.4$ 的二氧化硅,从而增大了折射率对比度。当光栅耦合器的光栅常数 $\Lambda > \lambda_0/n_{\text{eff}}$ ( $n_{\text{eff}}$ 为光栅耦合器的有效折射率)时,光波以偏离 $y$ 轴方向的 $\theta$ 角度入射,经过光栅衍射作用后,光波将在波导中沿 $-x$ 轴方向传播。

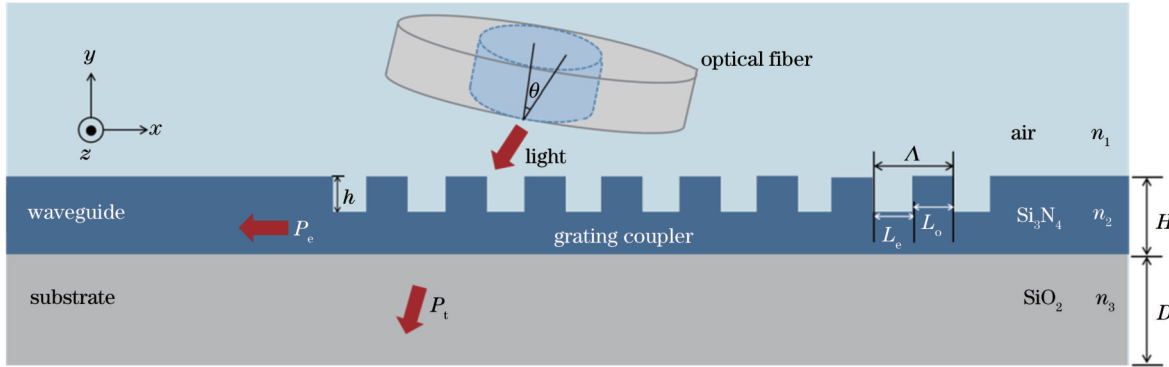


图1 二维光栅耦合器示意图

Fig. 1 Schematic diagram of two-dimensional grating coupler

在图1中,入射光通过光纤耦合进波导中,其中一部分光能在波导中稳定传播,即 $P_e$ ,另一部分光传播到衬底中,即 $P_t$ 。光栅的刻蚀深度为 $h$ ,刻蚀宽度为 $L_e$ ,未刻蚀宽度为 $L_o$ ,且 $\Lambda=L_e+L_o$ ,光栅的填充因子 $F_f$ 表示了未刻蚀宽度与光栅常数的比值<sup>[17]</sup>,即 $F_f=L_o/\Lambda$ 。光栅耦合器的有效折射率 $n_{\text{eff}}$ 取决于光栅耦合器的结构,由刻蚀部分的折射率 $n_e$ 和未刻蚀部分的折射率 $n_o$ 表示<sup>[9]</sup>,即

$$n_{\text{eff}} = F_f n_o + (1 - F_f) n_e. \quad (2)$$

刻蚀高度 $h$ 会影响 $n_e$ , $n_e$ 会随 $h$ 的增大而减小;刻蚀宽度会影响填充因子, $F_f$ 会随 $L_e$ 的增大而减小,进而影响 $n_{\text{eff}}$ 。光纤中的入射光波以 $\theta$ 角进入光栅耦合器,耦合光的传播方向沿着 $-x$ 轴,光波随后进入波导中。此时,布拉格方程可变为

$$\frac{2\pi n_{\text{eff}}}{\lambda_0} = \frac{2\pi n_1}{\lambda_0} \sin \theta + \frac{2\pi}{\Lambda}, \quad (3)$$

对式(3)进行变形,光栅常数可表示为 $\Lambda=\frac{\lambda_0}{n_{\text{eff}} - n_1 \sin \theta}$ 。根据式(3),当入射光波长与角度均确定时,可以计算出光栅常数的取值范围。但要注意的是,刻蚀高度 $h$ 、刻蚀宽度 $L_e$ 均会影响光栅常数的取值,在结构设计时,要考虑两者的影响。在本次设计中,光栅耦合器的耦合效率 $\eta$ 定义为波导端面接收到的功率 $P_{\text{out}}$ 与入射光源的功率 $P_{\text{in}}$ 之比,即

$$\eta = P_{\text{out}}/P_{\text{in}}. \quad (4)$$

## 2.2 结构设计

本文中主要考虑将一级衍射光波耦合进波导。为了保证TM模式的传播,波导层的高度 $H$ 必须大于TM模的截止厚度 $t$ <sup>[18]</sup>。对于TM模式, $t$ 可表示为

$$t = \frac{m\pi + \arctan\left(\frac{n_3^2 - n_1^2}{n_2^2 - n_3^2}\right)^{0.5}}{k(n_2^2 - n_3^2)^{0.5}}, \quad (5)$$

式中: $k=2\pi n_2/\lambda_0$ 。当入射光波长为785 nm、 $m=1$ 时, $t=108.19$  nm。为了便于计算,假设填充因子 $F_f=0.5$ ,刻蚀高度 $h=H/2$ ,此时, $n_{\text{eff}}=1.98$ , $\lambda_0/n_{\text{eff}}=397.47$  nm,因此 $\Lambda>397.47$  nm。在本次设计中,希望将一阶衍射光耦合进波导中,因此光源入射角度不宜过大。根据前期实验,选定光源入射角 $\theta \approx 10^\circ$ , $\Lambda=0.47$  μm。

## 3 结果与分析

### 3.1 二维光栅耦合器仿真与优化

FDTD仿真是利用空间离散化和有限差分来求解麦克斯韦方程组。本次仿真的主要目的是有效地探索光源入射角度、光栅常数、光栅高度、填充因子和刻蚀深度各参数的最佳值。

首先,对二维平面光栅耦合器进行研究分析。将光源固定在光栅耦合器上方1.59 μm和右边3.09 μm处,光栅常数、光栅高度、填充因子和光栅刻蚀深度的初始值分别定为0.47 μm、0.26 μm、0.50和0.13 μm。激励光波入射角度对耦合效率的影响如图2(a)所示,当入射角度为9°时,耦合效率最高,约为36%。当入射角度过大时,高级次的衍射光会进入波导中。根据衍射原理,衍射级次越大,衍射光的能量越低,因此耦合效率会降低。当入射角过小时,进入波导中的光可能是零级衍射光。

其他参数保持不变,激励光源的入射角度为9°,填充因子 $F_f$ 对耦合效率的影响如图2(b)所示。当

$F_f=0.514$ 时,耦合效率最高,约为39%。基于同样的仿真过程,得到刻蚀深度 $h$ 、光栅高度 $H$ 和光栅常数 $\Lambda$ 对耦合效率的影响如图2(c)所示。当 $h=0.132\mu\text{m}$ 、 $H=0.260\mu\text{m}$ 、 $\Lambda=0.455\mu\text{m}$ 时,耦合效率最高,约为39%; $h$ 过小会降低折射率对比度,进而降低耦合强度;当 $h$ 增大时,折射率对比度和耦合强度都得到提高,但光栅的反射率也提高了,从而也会导致耦合效率

降低。光栅常数与入射角共同决定了衍射级次,当衍射级次为1、光源入射角度为9°时,根据仿真分析, $\Lambda=0.455\mu\text{m}$ 时,光栅耦合器的耦合效率最高。

根据上述的参数扫描及优化,光栅耦合器的耦合效率 $\eta_1\approx39.64\%$ 。为了更形象地展示光栅耦合器的耦合作用,截取了优化光栅耦合器的电场分布,如图2(d)所示,光源进入耦合器之后,沿着 $-x$ 轴方向进入波导中。

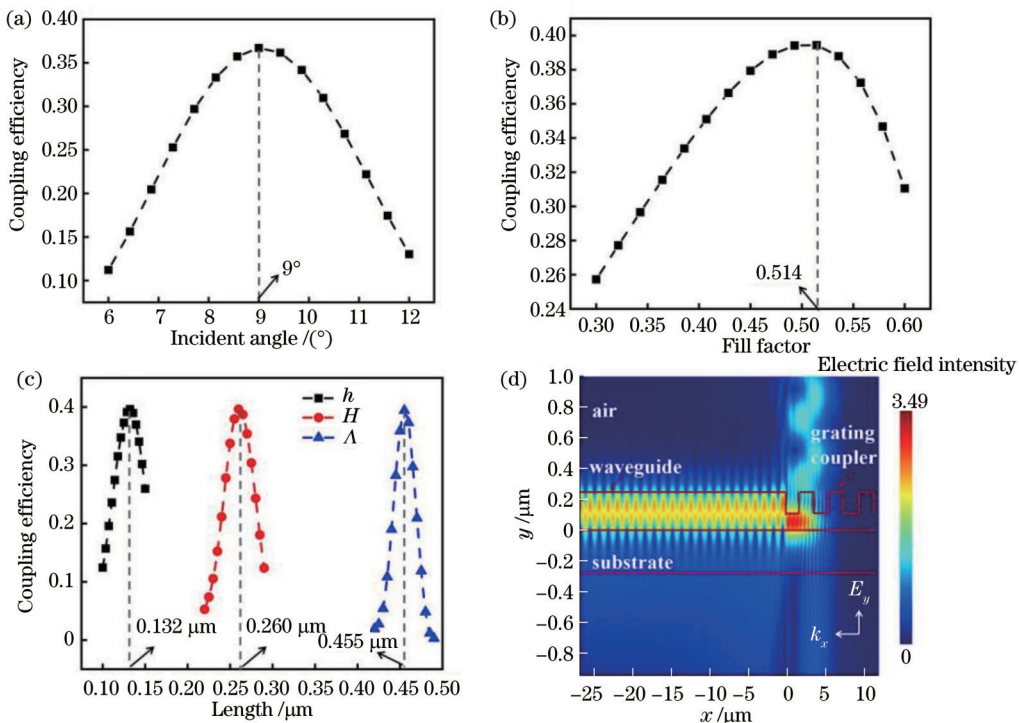


图2 各参数对耦合效率的影响及光栅耦合器电场分布图。(a)耦合效率随入射角度的变化;(b)耦合效率随填充因子的变化;(c)耦合效率随光栅刻蚀深度、光栅高度和光栅常数的变化;(d)二维光栅耦合器电场分布图

Fig. 2 Effect of various parameters on coupling efficiency and electric field distribution of grating coupler. (a) Coupling efficiency varying with angle of incidence; (b) coupling efficiency varying with fill factor; (c) coupling efficiency varying with grating etching depth, grating height, and grating constant; (d) electric field profiles of 2D grating coupler

### 3.2 三维光栅耦合器仿真与优化

以上述二维光栅耦合器的优化结果为基础,建立

了三维光栅耦合器的结构模型,如图3所示。

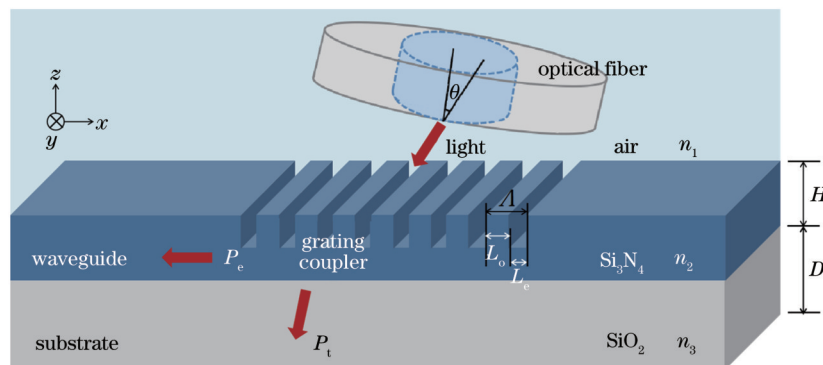


图3 三维直波导光栅耦合器示意图

Fig. 3 Schematic diagram of 3D direct waveguide grating coupler

三维直波导光栅耦合器、三维半刻蚀聚焦波导光栅耦合器和三维全刻蚀聚焦波导光栅耦合器的结构优

化参数如表1所示,其光场分布分别如图4(a)~(f)所示。

表1 三维波导光栅耦合器的结构优化参数  
Table 1 Structural optimization parameters of 3D waveguide grating couplers

Type of 3D grating coupler	Angle of incidence $\theta /(^{\circ})$	Height of grating coupler $H / \text{nm}$	Etching depth $h / \text{nm}$	Grating constant $\Lambda / \text{nm}$	Fill factor $F_f$	Width of waveguide $w / \text{nm}$	Angle of grating coupler $\theta /(^{\circ})$
3D direct type	6.05	256	152	478	0.40	1000	—
3D half etched and focused type	6.78	256	163	480	0.43	500	22
3D fully etched and focused type	10.96	303	303	533	0.71	500	22

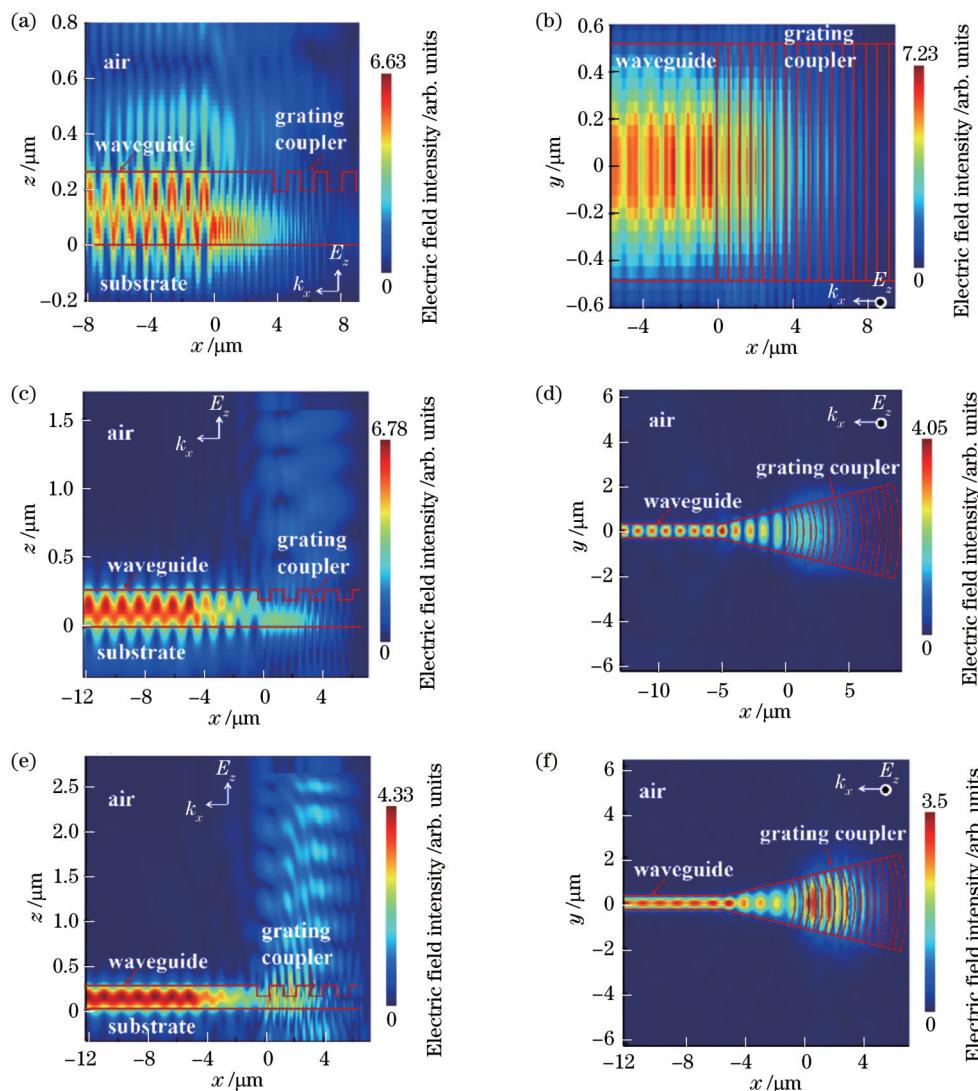


图4 光栅耦合器的xz与xy面电场分布图。(a)(b)三维直波导光栅耦合器;(c)(d)三维半刻蚀聚焦波导光栅耦合器;(e)(f)三维全刻蚀聚焦波导光栅耦合器

Fig. 4  $xz$  and  $xy$  surface electric field profiles of grating coupler. (a)(b) 3D direct waveguide grating coupler; (c)(d) 3D half etched and focused waveguide grating coupler; (e)(f) 3D fully etched and focused waveguide grating coupler

根据仿真分析,三维直波导光栅耦合器的耦合效率  $\eta_2=23.43\%$ ,半刻蚀聚焦波导光栅耦合器的耦合效率  $\eta_3=37.52\%$ ,聚焦全刻蚀波导光栅耦合器的耦合效率  $\eta_4=21.29\%$ 。相比于直波导光栅耦合器,聚焦光栅耦合器减小了耦合器的结构尺寸,同时保证了较低的模式转换损耗<sup>[19]</sup>。聚焦光栅耦合器的弧形光栅沟道都聚焦在波导和耦合器的连接之处,它可以将耦合光聚

焦到波导层中,实现了光纤与波导的高效耦合<sup>[20]</sup>。这里需要说明的是,本文的仿真分析基于785 nm的激励光波,在优化的结构参数条件下,聚焦光栅耦合器的耦合效率低于二维直波导光栅耦合器,略高于三维直波导光栅耦合器。全刻蚀和半刻蚀聚焦光栅的耦合效率出现差异的主要原因是:由于对全刻蚀聚焦波导光栅耦合器进行了全刻蚀处理,一个光栅周期包括一定宽

度的氮化硅和高度低一些的一定宽度的二氧化硅;半刻蚀聚焦波导光栅耦合器的一个光栅周期包括一定宽度的氮化硅和高度低一些的一定宽度的氮化硅。氮化硅的反射率稍高于二氧化硅的反射率,这对光栅的耦合效率有一定的提高作用。另外,全刻蚀和半刻蚀带来的聚焦光栅区域的有效折射率不一样,这也会对耦合效率产生一定的影响。

### 3.3 三维聚焦全刻蚀波导光栅耦合器的测试

受工艺手段的限制,利用电子束光刻法加工制备了三维聚焦全刻蚀波导光栅耦合器,氮化硅波导加工流程如图5所示,光栅耦合器的结构参数如表2所示,其SEM表征如图6所示。

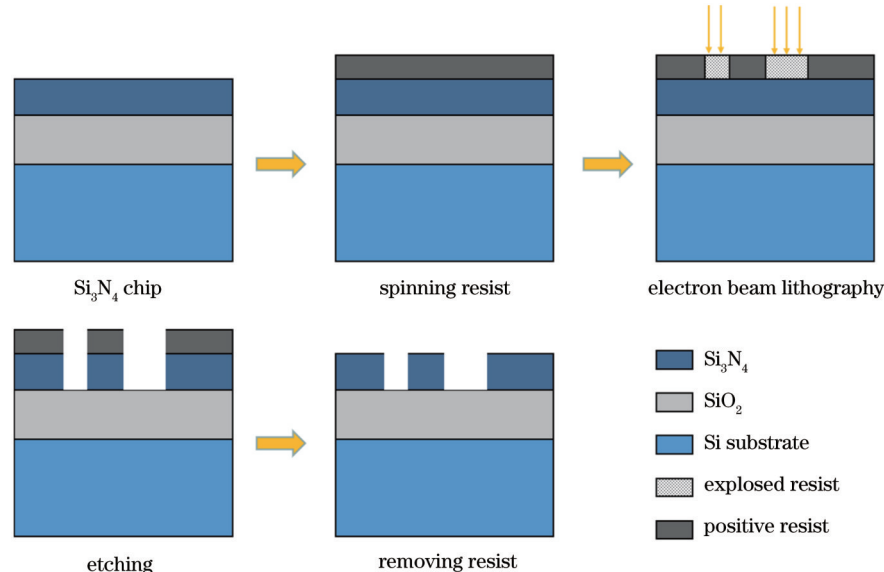


图5  $\text{Si}_3\text{N}_4$ 波导制作流程

Fig. 5 Production process of  $\text{Si}_3\text{N}_4$  waveguide

表2 三维全刻蚀聚焦波导光栅耦合器的结构优化参数

Table 2 Structural optimization parameters of 3D fully etched and focused waveguide grating coupler

Angle of grating coupler $\theta /(^{\circ})$	Etch depth $h / \text{nm}$	Grating constant $\Lambda / \text{nm}$	Fill factor $F_f$	Width of waveguide $w / \text{nm}$
22	300	670	0.78	150

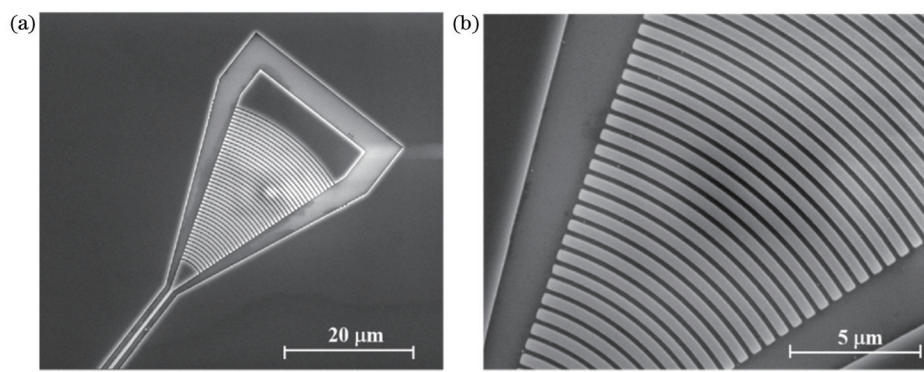


图6 三维全刻蚀聚焦波导光栅耦合器SEM图像。(a)全貌图;(b)刻蚀结构

Fig. 6 SEM images of 3D fully etched and focused waveguide grating coupler. (a) Overall view; (b) etching structure

三维全刻蚀聚焦波导光栅耦合器的测试系统如图7所示,系统的主要光学器件包括安扬激光(TSL)的SC-PRO-M型超连续谱光源、可调窄带滤波器(可以对输入光波长进行选择)、鑫锐光SMA的9  $\mu\text{m}$ /125  $\mu\text{m}$ 光纤(作为输入/输出光纤)和AQ6370D光谱仪(采集输出光谱信号)。通过对光谱信号在一定波长

范围内的积分可以获得光功率,再进行耦合效率的计算。在测量过程中,光源经过可调窄带滤波器后,光纤将输入光耦合到光栅耦合器,输入光经过氮化硅直波导,光栅耦合器将输出光耦合到接收光纤中,最后将光传到光谱仪中进行测量。

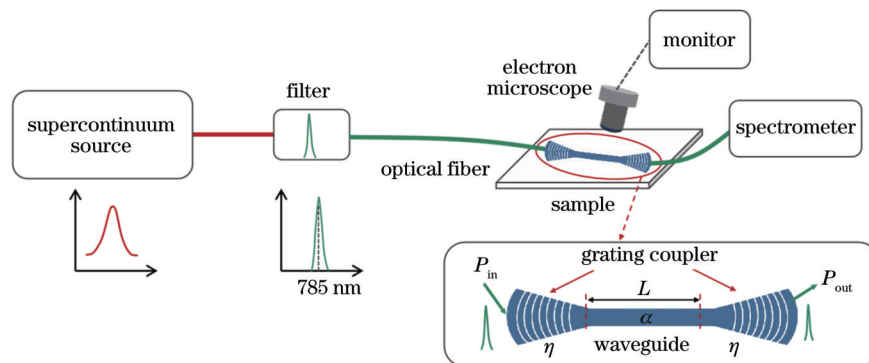


图7 光栅耦合器测试系统图

Fig. 7 Test system diagram of grating coupler

由于光纤传输损耗较小,进入光栅耦合器的光功率可近似等于光源发出的光功率,因此,可以得到出射光功率 $P_{\text{out}}$ 与入射光功率 $P_{\text{in}}$ 的关系为

$$P_{\text{out}} = P_{\text{in}} \times \eta^2 \times 10^{-\alpha L}, \quad (6)$$

式中: $\eta$ 是光栅耦合器的耦合效率; $\alpha$ 是氮化硅直波导的损耗系数; $L$ 是氮化硅直波导的长度。当保持光源持续输出及平台稳定时, $P_{\text{in}}$ 不变。由此可得 $\alpha$ 的计算公式为

$$\alpha = \frac{10 \lg \left( \frac{P_{\text{out}2}}{P_{\text{out}1}} \right)}{L_1 - L_2}, \quad (7)$$

式中: $P_{\text{out}1}$ 是直波导长度为 $L_1$ 时的输出; $P_{\text{out}2}$ 是直波导长度为 $L_2$ 时的输出。

首先制备了不同长度的直波导器件,以测试氮化硅波导的损耗系数。测试时保持光源、光入射角度、光谱仪等其他测试条件完全相同,测得不同长度的氮化硅波导的传播损耗如图8所示,经过拟合处理得到了氮化硅波导的损耗系数 $\alpha = 1.267 \text{ dB/mm}$ 。制备过程中会导致晶圆残渣或胶残留在样品上,从而增大了氮化硅波导的损耗,导致波导损耗系数偏大。后续可以进一步优化工艺处理过程。

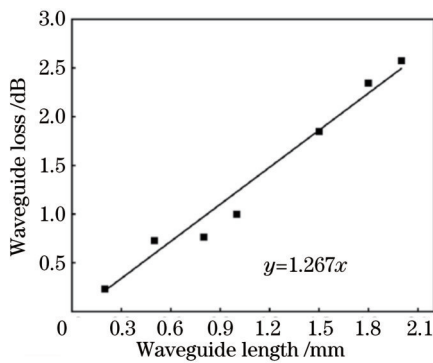


图8 波导损耗随波导长度的变化曲线图

Fig. 8 Plot of waveguide loss varying with waveguide length

光栅耦合器的耦合效率 $\eta$ 的计算表达式为

$$\eta = \left( \frac{P_{\text{out}}}{P_{\text{in}}} \times 10^{\alpha L} \right)^{\frac{1}{2}}. \quad (8)$$

接着,选用 $L=200 \mu\text{m}$ 的直波导进行测试。在测试过程中,保持其他测试条件不变,通过可调窄带滤波器改变耦合输入光的波长,进行光谱带宽测试,测试得到的光栅耦合器对不同波长光波的耦合效率如图9所示。保持光源持续输出和各测试条件不变,通过可调窄带滤波器输出785 nm波长的光,制备的全刻蚀聚焦光栅耦合器的耦合效率测试结果如表3所示。

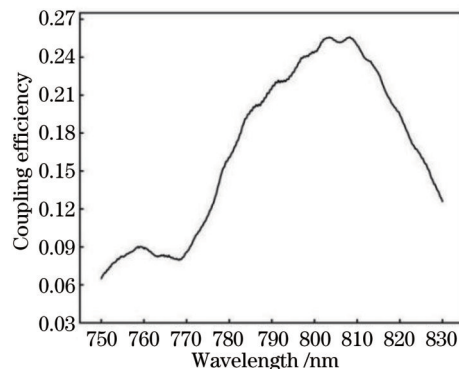


图9 光栅耦合器的光谱带宽测试结果

Fig. 9 Test result of spectral bandwidth of grating coupler

表3 全刻蚀聚焦耦合光栅对785 nm光的耦合效率测试结果

Table 3 Test results of coupling efficiency of fully etched and focused coupling grating at 785 nm

Test	Incident optical power $P_{\text{in}} / \text{mW}$	Emergent light power $P_{\text{out}} / \mu\text{W}$	Coupling efficiency $\eta / \%$
1	1.5	32.80	19.80
2	1.5	32.64	19.75
3	1.5	33.12	19.89
4	1.5	33.76	20.08
5	1.5	33.60	20.04

根据表3,可得平均耦合效率约为19.91%。测试结果和上述仿真结果相比有略微差别,其主要原因在于制备工艺误差导致光栅耦合器的表面不完全平整,使得仿真模型和实际测试结构有所偏差,从而影响光栅耦合器的耦合效率。

## 4 结 论

对2D、3D氮化硅波导光栅耦合器进行了数值分析和优化，并进行了器件加工和性能测试研究。结果表明：2D波导光栅耦合器的性能最好，其耦合效率可达39.64%；3D全刻蚀聚光栅耦合器在实际测试中的耦合效率能达约19.91%，能有效将光耦合进波导中。后续还可以在光栅耦合器的材料选择上和结构设计上进行优化，进一步提高光栅耦合器的耦合效率。

## 参 考 文 献

- [1] Halir R, Ortega-Monux A, Schmid J H, et al. Recent advances in silicon waveguide devices using sub-wavelength gratings[J]. IEEE Journal of Selected Topics in Quantum Electronics, 2014, 20(4): 279-291.
- [2] Zhang J J, Yang J B, Xin H, et al. Ultrashort and efficient adiabatic waveguide taper based on thin flat focusing lenses[J]. Optics Express, 2017, 25(17): 19894-19903.
- [3] 刘少平, 姜小明, 赖林, 等. 基于平板波导-金纳米颗粒基底的表面增强拉曼散射信号长程探测[J]. 激光与光电子学进展, 2021, 58(23): 2330003.  
Liu S P, Jiang X M, Lai L, et al. Long-range detection of surface-enhanced Raman scattering signal based on flat-plate waveguide-gold nanoparticles substrate[J]. Laser & Optoelectronics Progress, 2021, 58(23): 2330003.
- [4] 赵然, 孙崇磊, 徐晓, 等. 基于亚波长光栅的高集成度垂直光耦合器[J]. 光学学报, 2020, 40(14): 1405002.  
Zhao R, Sun C L, Xu X, et al. Ultra-compact vertical optical coupler based on subwavelength grating[J]. Acta Optica Sinica, 2020, 40(14): 1405002.
- [5] 刘萌, 郑煊, 刘文斐, 等. 基于亚波长线光栅的垂直光栅耦合器的设计[J]. 激光与光电子学进展, 2021, 58(17): 1705002.  
Liu M, Zheng X, Liu W F, et al. Design of vertical grating coupler based on sub-wavelength line gratings[J]. Laser & Optoelectronics Progress, 2021, 58(17): 1705002.
- [6] Sacher W D, Huang Y, Ding L, et al. Wide bandwidth and high coupling efficiency Si<sub>3</sub>N<sub>4</sub>-on-SOI dual-level grating coupler[J]. Optics Express, 2014, 22(9): 10938-10947.
- [7] Benedekovic D, Cheben P, Schmid J H, et al. High-efficiency fully etched fiber-chip grating couplers with subwavelength structures for datacom and telecom applications[J]. Proceedings of SPIE, 2015, 9516: 95160I.
- [8] Gao Y, Liu Y F, Liao J L, et al. Study on angle detection capability of silicon waveguide grating coupler[J]. Proceedings of SPIE, 2018, 10848: 1084807.
- [9] Larrea R, Gutierrez A M, Sanchis P. Design method for high performance grating couplers in photonic integrated circuits[J]. Optical and Quantum Electronics, 2018, 50(9): 341.
- [10] Hong J X, Qiu F, Spring A M, et al. Silicon waveguide grating coupler based on a segmented grating structure[J]. Applied Optics, 2018, 57(12): 3301-3305.
- [11] Xu Y, Wang F, Gao Y, et al. Efficient polymer waveguide grating coupler with directionality enhancement[J]. Optics Communications, 2020, 463: 125418.
- [12] van Laere F, Claes T, Schrauwen J, et al. Compact focusing grating couplers for silicon-on-insulator integrated circuits[J]. IEEE Photonics Technology Letters, 2007, 19(23): 1919-1921.
- [13] Zhao X J, Li D P, Zeng C, et al. Compact grating coupler for 700-nm silicon nitride strip waveguides[J]. Journal of Lightwave Technology, 2016, 34(4): 1322-1327.
- [14] Cheng L R, Mao S M, Wang Y H, et al. Fiber-chip bi-wavelength multiplexing with subwavelength single-etch grating coupler and diplexer[J]. IEEE Photonics Journal, 2022, 14(1): 2210706.
- [15] Rigler M, Troha T, Guo W, et al. Second-harmonic generation of blue light in GaN waveguides[J]. Applied Sciences, 2018, 8(8): 1218.
- [16] Marchetti R, Lacava C, Carroll L, et al. Coupling strategies for silicon photonics integrated chips[J]. Photonics Research, 2019, 7(2): 201-239.
- [17] Zhang Z Y, Huang B J, Zhang Z, et al. Highly efficient vertical fiber interfacing grating coupler with bilayer anti-reflection cladding and backside metal mirror[J]. Optics & Laser Technology, 2017, 90: 136-143.
- [18] Prokop C, Schoenhardt S, Laegel B, et al. Air-suspended SU-8 polymer waveguide grating couplers[J]. Journal of Lightwave Technology, 2016, 34(17): 3966-3971.
- [19] 梁宇鑫, 李智慧, 范诗佳, 等. 氮化硅低损耗光栅耦合器的设计与制备[J]. 光通信技术, 2022, 46(4): 68-72.  
Liang Y X, Li Z H, Fan S J, et al. Design and fabrication of the SiN grating coupler with low coupling loss[J]. Optical Communication Technology, 2022, 46(4): 68-72.
- [20] Waldhäusl R, Schnabel B, Dannberg P, et al. Efficient coupling into polymer waveguides by gratings[J]. Applied Optics, 1997, 36(36): 9383-9390.

## Optimization and Experiments of On-Chip Silicon Nitride Grating Couplers

Ran Na, Chen Xinyang, Wang Zhengkun, Zhang Jie\*

*Key Laboratory of Optoelectronic Technology & Systems, Ministry of Education, Chongqing University,  
Chongqing 400044, China*

### Abstract

**Objective** The integration of Raman spectroscopy detection system is the current focus of Raman technology, especially combining waveguide with Raman, and effectively coupling excitation light into waveguide is particularly important for Raman spectroscopy sensing and signal collection. The process is mainly realized by waveguide grating couplers. However, the majority of the waveguide grating couplers are studied for the C band. In addition, the physical designs of the grating couplers are very complex and the preparation processes are difficult. The transparent window of the silicon

nitride used in this paper is between 400 nm and 3500 nm. It has a wide range and a high refractive index, which can form a refractive index difference with the surrounding materials to bind the energy of the light in the waveguide layer, and it can reduce the transmission loss of light in the waveguide. The grating coupler designed here has a simple structure and preparation process. Besides, the wavelength of excitation light is 785 nm, which is also commonly used in Raman sensing. The grating couplers studied here can effectively couple the excitation light into the waveguide, and it is helpful for Raman spectroscopy sensing and signal collection.

**Methods** Firstly, we have a theoretical analysis based on the principle of the grating coupler and analyze the interaction of parameters and the effect of each parameter on the coupling efficiency. Then the two-dimensional and three-dimensional models of the grating couplers are established, and the finite difference time domain (FDTD) simulation software is used to analyze them. With coupling efficiency as the main performance index, the influences of incident angle, grating constant, grating height, filling factor, and etching depth are analyzed to achieve the maximum of the coupling efficiency of the grating couplers. Electron beam lithography is used to prepare three-dimensional fully etched and focused waveguide grating couplers and an optical system including a supercontinuum source, tunable narrow bandpass filters which can select the wavelength of incident light, optical fibers which are used as the input and output fibers, and a spectrometer which collects output spectral signal is built. Then the prepared grating couplers are tested experimentally. In the test, direct waveguide devices of different lengths are prepared to test the loss factor of silicon nitride waveguide, and the test conditions such as light source, angle of incidence, and spectrometer are kept exactly the same. Next, the coupling efficiency of the grating coupler is tested. After the laser from the light source passes through the tunable narrow bandpass filter, the optical fiber couples the incident light into the grating coupler, the input light passes through the silicon nitride direct waveguide, then the grating coupler couples the light into the output optical fiber, and the output light is transmitted to the spectrometer for measurement. Finally, the coupling efficiency of the grating couplers is calculated according to the relationship of power of emergent light and incident light.

**Results and Discussions** In the simulation analysis, for the two-dimensional grating coupler, the final optimization value for the grating constant, grating height, filling factor, and etching depth are  $0.455\text{ }\mu\text{m}$ ,  $0.260\text{ }\mu\text{m}$ ,  $0.514$ , and  $0.132\text{ }\mu\text{m}$ , respectively. The coupling efficiency of the final two-dimensional grating coupler is about 39.64% (Fig. 2). The coupling efficiencies of three-dimensional direct waveguide grating coupler, three-dimensional half etched and focused waveguide grating coupler, and three-dimensional fully etched and focused waveguide grating coupler are 23.43%, 37.52%, and 21.29% (Fig. 4), respectively. Compared to the direct waveguide grating coupler, the focused grating coupler has a smaller structural size, while ensuring a lower mode conversion loss. All the grating trenches of the focused waveguide grating coupler are focused on the junction between the waveguide and the grating coupler, which can focus the coupled light into the waveguide layer. The efficient coupling between the optical fiber and waveguide is realized. In the experimental test, firstly, the loss factor of the silicon nitride waveguide is tested. Then the light source and test conditions remain constant, and the light is transmitted to the spectrometer for measurement finally. The coupling efficiency of the three-dimensional fully etched and focused grating coupler can reach about 19.91% (Table 3). The reason for the different coupling efficiencies between experimental test results and simulation results is that the surface of the actual grating couplers is not completely flat due to the matching error in the process of fabricating the grating couplers. So there is a little difference between the simulation models and the samples in the test, and thus the coupling efficiency of the grating coupler in the experimental is slightly lower.

**Conclusions** In this paper, the finite difference time domain (FDTD) simulation software is used to analyze and optimize the two-dimensional and three-dimensional silicon nitride waveguide grating couplers. The three-dimensional fully etched and focused waveguide grating couplers are prepared by electron beam lithography, and the performance of grating couplers is tested. The results show that the performance of the two-dimensional grating coupler whose coupling efficiency is 39.64% is the best, and the coupling efficiency of three-dimensional fully etched and focused waveguide grating coupler in the experiment 19.91%, which can couple light into the waveguide effectively. The material selection and structure design of the grating couplers can also be optimized to improve the coupling efficiency of the grating couplers in the future.

**Key words** integrated optics; grating coupler; silicon nitride waveguide; structural optimization; coupling efficiency